Size-resolved physico-chemical characterization of diesel exhaust particles and efficiency of exhaust aftertreatment

Zeraati Rezaei, Soheil; Alam, Salim; Xu, Hongming; Beddows, David; Harrison, Roy

DOI:
10.1016/j.atmosenv.2019.117021

Document Version
Peer reviewed version

Citation for published version (Harvard):
Zeraati Rezaei, S, Alam, S, Xu, H, Beddows, D & Harrison, R 2020, 'Size-resolved physico-chemical characterization of diesel exhaust particles and efficiency of exhaust aftertreatment', *Atmospheric Environment*, vol. 222, 117021. https://doi.org/10.1016/j.atmosenv.2019.117021

Size-Resolved Physico-Chemical Characterization of Diesel Exhaust Particles and Efficiency of Exhaust Aftertreatment

Soheil Zeraati-Rezaei[1], Mohammed S. Alam[2], Hongming Xu[1], David C. Beddows[2,3] and Roy M. Harrison[2,3*†]

[1] Department of Mechanical Engineering
School of Engineering, University of Birmingham, Edgbaston
Birmingham, B15 2TT
United Kingdom

[2] School of Geography, Earth & Environmental Sciences
University of Birmingham, Edgbaston, Birmingham, B15 2TT
United Kingdom

[3] National Centre for Atmospheric Science
School of Geography, Earth and Environmental Sciences
University of Birmingham
Edgbaston, Birmingham B15 2TT
United Kingdom

[*] To whom correspondence should be addressed.
Tele: +44 121 414 3494; Fax: +44 121 414 3708; Email: r.m.harrison@bham.ac.uk

[†] Also at: Department of Environmental Sciences / Center of Excellence in Environmental Studies, King Abdulaziz University, PO Box 80203, Jeddah, 21589, Saudi Arabia

HIGHLIGHTS

- Particle emissions sampled from a light-duty diesel engine
- Size fractionated from <10 nm to >10 µm diameter and then chemically characterized
- Hydrocarbons peak at 100 nm and are alkanes (main), cyclics, bicyclics, aromatics
- Hydrocarbons removed by >90% by DOC+DPF while oxygenates formed within DOC+DPF
- High concentration of <2.5 nm particles measured and efficiently removed by DOC+DPF

ABSTRACT

Knowledge of physico-chemical characteristics of particle emissions from combustion engines is essential for various modelling purposes and environmental analysis. It is of particular interest to obtain emission factors of intermediate-volatility organic compounds (IVOC) and semi-volatile organic compounds (SVOC) which have not been comprehensively reported in the literature due to the limitations of characterisation methods. In the current study, a multi-stage Nano impactor and the two-dimensional gas chromatography (GC×GC) mass spectrometry (MS) technique were used to comprehensively characterise size fractionated particle phase emissions from a light-duty diesel engine based on the particle size, compound groups and carbon number. The number size distributions of particles between 1.2-1000 nm were also investigated. Exhaust gas samples were taken before a diesel oxidation catalyst (DOC), after the DOC and after the DOC combined with a catalysed diesel particulate filter (DPF). In samples taken before the DOC (engine-out), the total particulate IVOC+SVOC (I+SVOC) emission factor was approximately 105 milligrams per kilogram of fuel consumed (which was ~49% of the total particle mass) and the peak concentration of different classes of I+SVOC was found in the particle size bins close to 100 nm where most of the total particle mass was found. Alkanes, with maximum abundance at C_{24}, were the most dominant class of I+SVOC in samples taken before and after the aftertreatment devices. Total particulate I+SVOC emissions were removed with ~75% efficiency using the DOC and by ~92% using the DOC+DPF. Alkanes, cycloalkanes, bicyclics and monoaromatics were all removed by >90% using the DOC+DPF; however, oxygenates were removed by only ~76% presumably due to the oxidation of different species within the aftertreatment system and reappearance as oxygenates. A high concentration of particles was measured in the sub-2.5 nm range. These particles were efficiently removed by the DOC+DPF due to both the loss of I+SVOC and physical filtration.

Key words: Diesel engine; Particulate matter; Particle size magnifier; SVOC; DOC; DPF;

1. INTRODUCTION

Adverse environmental and health effects of primary and secondary emissions originated from combustion engines have motivated research into their properties and possible abatement mechanisms. Conventionally, diesel compression ignition engines are more energy efficient (emit less CO_2) compared to their gasoline spark ignition engine counterparts (Heywood, 1988; Stone, 1999). This has resulted in widespread utilisation of diesel engines for heavy-duty and light-duty applications; currently in Europe approximately half of the road vehicles are diesel fuelled (IEA, 2016; ICCT, 2018), even though there has been a recent decline in the number of newly registered diesel vehicles (ICCT, 2018; Department for Transport UK, 2018). However, conventional diesel vehicles with no or malfunctioning aftertreatment systems can emit higher levels of oxides of nitrogen (NO_x) and particulate matter compared to gasoline vehicles. There still can be some challenges for the modern diesel aftertreatment systems to operate efficiently under certain operating conditions. For instance, NO_x abatement in the fuel-lean exhaust of diesel vehicles can be problematic at low exhaust temperatures (Majewski and Khair, 2006), and the impact of active regeneration of a diesel particulate filter (DPF) on deteriorating engine fuel economy and increasing vehicle emissions (including particulate matter itself) can be considerable (Majewski and Khair, 2006; Gordon et al., 2014).

Emissions of particles, the pollutant with the greatest public health impact (IEA, 2016), contain mostly elemental carbon and organic compounds (Eastwood, 2008; Kittelson, 1998). The organic fraction is complex as it derives from thousands of different hydrocarbons (HC) in unburned fuel and engine lubricating oil and contains compounds resulting from partial combustion and pyrolysis (Funkenbusch et al., 1979; Black and High, 1979; Alam et al., 2016; Zeraati-Rezaei et al., 2016; Laurence et al., 1996). Typical European diesel fuels and engine lubricating oils are mainly comprised of intermediate–volatility organic compounds (IVOC) and semi-volatile organic compounds (SVOC) in the range of C_{11} to C_{30} (fuel) and C_{16} to C_{33} (oil) (Alam et al., 2018). Gas-

particle partitioning of the IVOC+SVOC (I+SVOC), with different volatilities and vapour pressures, is highly active under the exhaust conditions (Alam et al., 2016; Donahue et al., 2006), with at least one percent of the SVOC mass being found in either the condensed or gas phase (Donahue et al., 2006). Their vapour pressure in the atmosphere is between 10^{-11} and 10^{-5} atm and compounds in the exhaust of on-road diesel vehicles can contribute to the formation of secondary organic aerosol (SOA) (Gordon et al., 2014; Zhao et al., 2015; Drozd et al., 2019). This highlights the importance of knowing their detailed composition and concentration within the engine exhaust.

In this paper, the terms primary emissions and primary organic aerosol (POA) refer to pollutants which exit the tailpipe, or are produced by processing in ambient air within a few seconds of emission, such as the particles formed by nucleation of hot vapours as emissions dilute in roadside air (Charron and Harrison, 2003). This differentiates them from secondary pollutants which form from chemical reactions in the atmosphere on a longer timescale.

Studies, such as those by Huang et al. (2015) and Sakurai et al. (2003), have shown that the organic fraction of particles is composed of compounds such as normal and branched alkanes, alkyl-cycloalkanes, various aromatics and polycyclic aromatic hydrocarbons (PAH). However, few studies have addressed SVOC with large carbon numbers (C>15) in a detailed quantitative manner since they are largely unresolved by conventional gas chromatography (GC) techniques and create an unresolved complex mixture (UCM) in the chromatogram (Alam et al., 2016). Zhao et al. (2015) claimed that on average more than 90% of compounds with approximately similar effective saturation concentrations to those of C_{12} to C_{22} n-alkanes (i.e. between 10^3 and 10^6 $\mu g/m^3$) appeared as a UCM in conventional GC mass spectrometry (MS) techniques. However, using a more comprehensive technique, such as two-dimensional GC (GC×GC), helps to overcome this issue. Alam et al. (2018) conducted a comprehensive study on diesel I+SVOC emissions using GC×GC

time of flight (ToF) MS and were able to characterise each major I+SVOC class according to the carbon number.

Gordon et al. (2014) conducted environmental chamber experiments to investigate SOA formation from the diluted exhaust of medium- and heavy-duty diesel vehicles (the minimum engine displacement volume was 5.9 L). They reported that knowledge of the uncharacterised less volatile species in the UCM (~30% of the non-methane organic gas emissions) is necessary to better understand SOA formation. Characterising these species can also lead to more accurate emission factors. Total POA emission factors of below 100 mg/kg_f (milligrams per kilogram of fuel consumed) were reported for the vehicles with no exhaust aftertreatment. These emission factors were calculated under the assumption that all carbon in the fuel is converted to CO_2 (Gordon et al., 2014). Actual measurements of engine fuel consumption can be helpful in improving the accuracy of normalising the emission concentrations.

Some studies have shown that I+SVOC emission factors are strongly influenced by the exhaust aftertreatment technology installed on the vehicle (Gordon et al., 2014; Zhao et al., 2015; Liu et al., 2018; May et al., 2013). Liu et al. (2018) reported that the soluble organic fraction of particle emissions from a large (8.9 L) non-road diesel engine was decreased by >80% when using a diesel oxidation catalyst (DOC) in combination with a selective catalytic reduction system (SCR) and a DPF. They suggested that a large fraction of SVOC is possibly in the gas phase under exhaust conditions and is influenced by the DOC. Gordon et al. (2014) found that primary particle emissions and SOA formation in the diluted exhaust of medium-heavy duty diesel vehicles equipped with a catalysed DPF were very small under normal operation. However, during active DPF regeneration, significant amounts of primary particles and SOA formation were measured. SOA concentrations in the diluted exhaust of some vehicles with no DPF were more than two times that of POA. Studies on light-duty diesel vehicles are very limited; May et al. (2013) recommended

investigating the volatility distribution of I+SVOC emissions from the light-duty diesel vehicles widespread in Europe.

The majority of POA emissions from diesel vehicles are believed to be semi-volatile (May et al., 2013); therefore, they are likely to shrink in size as a result of evaporation in the atmosphere due to high dilution and long residence time (Robinson et al., 2007; Dall'Osto et al., 2011). It has been shown that atmospheric-like dilution of the exhaust of diesel vehicles with no DPF causes one-half to two-thirds of the POA to evaporate (May et al., 2013). However, the composition and concentration of I+SVOC in each size class of engine exhaust particles have not previously been reported comprehensively in the literature. Size-resolved chemical composition data can be particularly useful and essential for:

- determining gas transfer effects on the atmospheric evolution of emitted engine particles on different scales (for example in the study conducted by Nikolova et al. (2018) on the neighbourhood scale;
- understanding and modelling of particle evolution within the vehicle exhaust system, designing and modelling of oxidative and reductive catalysts as well as particulate filters.

"Another topic that has not been clearly covered in the available literature, is the study of very small particles with diameters <3 nm emitted from modern light-duty engines. Recently, these particles have been shown to be a major fraction of the total particle emissions measured in the atmosphere (Hietikko et al., 2018) which are sourced from road transportation (including both heavy-duty and passenger vehicles) and those emitted from a heavy-duty engine during engine laboratory experiments – emission factors as high as 4.3×10^{15} $(kg_{fuel})^{-1}$ were measured (Rönkkö et al., 2017). Järvinen et al. (2019) used a particle size magnifier (PSM) and investigated in-traffic emissions from city buses (including Euro VI compliant buses). They found that the studied buses can be sources of large concentrations of particles in the diameter range of 1.3-3 nm, even using

aftertreatment system, depending on the driving conditions. These very small particles emitted from different engines are believed to have both volatile and non-volatile constituents. Alanen et al. (2015) studied the formation and physical properties of the particle emissions from a natural gas engine including study of particles <3 nm with a PSM. They suggested that particles did not evaporate completely even at 265 °C and have non-volatile cores, although it should be mentioned that diesel engine particle emissions are very different from natural gas engine emissions. Even in less recent studies, the presence of non-volatile cores in the sub-3 nm particles was highlighted. Filippo and Maricq (2008) investigated the volatility of particle emissions larger than 2 nm in the exhaust of light-duty vehicles and reported that the nucleation mode particles remain non-volatile to >400 °C indicative of solid cores. The sources of these very small particles with presumably a solid core are assumed to be in high temperature regions inside or in the vicinity of the combustion chamber due to their electrical charge (Alanen et al., 2015; Sgro et al., 2012; Filippo and Maricq, 2008). It is important to investigate sub-3 nm particles emitted from modern light-duty diesel engines and obtain their emission factors as the picture is not clear for the fleet using these engines."

In the current paper, for the first time, size-resolved particle phase I+SVOC emission factors (concentrations normalised to the actual engine fuel consumption) for a light-duty diesel engine are comprehensively reported based on the compound type and carbon number using a multi-stage Nano impactor and GC×GC-ToF-MS technique. Furthermore, emission factors for CO, total HC (THC), NO, NO_2, NO_x, CO_2, particle mass and number are presented. Particle size distributions are characterised also in the sub-2.5 nm range using a PSM coupled with a condensation particle counter. The link between particle size distribution and presence of I+SVOC in each particle size bin is addressed. Furthermore, the individual effects of a DOC and a catalysed DPF on characteristics of gaseous and particle (including I+SVOC and sub-2.5 nm) emissions are investigated. Although engine and aftertreatment designs as well as fuel and lubricating oil

formulations are different around the world, presenting the results before and after these aftertreatment devices can help elucidate situations where there are no or limited exhaust aftertreatment systems installed in the vehicle.

2. EXPERIMENTAL SETUP

Experiments were conducted on a 2.2 L, 4-cylinder in-line diesel compression ignition (CI) engine equipped with a common rail direct-injection (DI) system and a variable-nozzle-turbine (VNT) turbocharger. This is a light-duty production engine, as found in the market designed for vehicles registered after 2011 (Euro 5), without any major changes to its original settings. Main specifications of the engine are listed in Table 1. The schematic of the engine dynamometer test cell is illustrated in Figure 1. The open engine control unit (Open-ECU) allows full control over the engine operating parameters.

Experiments were performed at the low engine load of 1.4 bar brake mean effective pressure (BMEP) and speed of 1800 revolutions per minute (RPM). This engine condition was selected from a dynamometer testing matrix used for assessing the engine performance and fuel economy in a target vehicle new European driving cycle (NEDC) test. Furthermore, I+SVOC characterisation at this condition is believed to be important as the formation rate of SOA from I+SVOC has shown to be higher in the diluted exhaust of engines operating at lower loads (Gordon et al., 2014). A pilot+main fuel injection strategy with an injection pressure of 600 bar was used and exhaust gas recirculation (EGR) was fixed at 33%. Experiments were conducted under the steady state engine condition – the engine was fully warmed-up and thermally stable.

The engine was equipped with a newly-fitted DOC+DPF exhaust aftertreatment system; the DOC was located upstream of the DPF. The honeycomb of the DOC has a circular profile with a diameter

of 144 mm and length of 96 mm and has 20×20 (400) cells per square inch. The DPF brick is 157 mm in length and has an oval cross section (188 mm and 153 mm in cross sectional profile). This DPF is believed to be catalysed as it oxidised unconverted exhaust CO and HC during the experiments. During these experiments, exhaust back pressure did not exceed the level at which it is required to use the active regeneration strategies. Active regeneration of the DPF is known to significantly increase primary particulate matter emissions and SOA formation (Gordon et al., 2014). However, it is necessary to identify the contribution of the active regeneration emissions to the total light-duty vehicle emissions; but this was out of the scope of the current study. Gordon et al. (2014) estimated this to be negligible for medium- and heavy-duty diesel vehicles by considering the regeneration frequency – total particulate matter filtration efficiency was reduced by less than 2%.

Ultra-low sulphur diesel fuel that complied with the EN590 specifications was used for these experiments – cetane number was 52.5 and sulphur content was approximately 8 mg/kg. This diesel fuel has been comprehensively analysed previously and results showed that it includes n-alkanes, branched alkanes (mono-, di-, tri-, tetra- and penta-methyl), n-alkyl cycloalkanes, branched monocyclic alkanes, C_1–C_{12} substituted bicyclic alkanes, C_1–C_4 substituted tetralins and indanes, C_3–C_{12} substituted monocyclic aromatics, C_1–C_3 substituted biphenyls/acenaphthenes, C_1–C_4 substituted bicyclic aromatics, C_1–C_2 substituted fluorenes, C_1–C_2 substituted phenanthrene/anthracenes and unsubstituted PAH (Alam et al., 2018). The majority of the compounds are aliphatic, and aromatic mass content is approximately 10% (Alam et al., 2018). Engine fuel mass consumption was measured by an AVL 733s dynamic fuel meter equipped with an AVL 752-60 fuel cooler. Fuel temperature in the feed and return lines was monitored and controlled to assure repeatable fuel consumption measurements. The fuel meter was calibrated frequently using a built-in function. Fuel consumption measurement error by the AVL 733s is from 0.12% to 0.2% of the measured values depending on the fuel consumption.

The utilised SAE 5W30 part-synthetic lubricating oil is representative of the standardised engine lubricating oils available in the market complying with the ACEA A1/B1 and API SN/CF oil industry standards and the WSS-M2C913-B vehicle manufacturer specifications. Characterisation results of the typical engine lubricating oils have been reported elsewhere (Alam et al., 2018; Liang et al., 2018). Briefly, a typical SAE 5W30 lubricating oil mainly contains C_{16}–C_{33} straight and branched chain alkanes, C_{16}–C_{33} monocyclic alkanes, C_{17}–C_{33} bicyclic alkanes, C_{17}–C_{33} tricyclic alkanes and C_{16}–C_{33} monocyclic aromatics (Alam et al., 2018).

Calibrated K-type thermocouples (RS Company), with mostly 3 mm probe diameter, were used to measure temperatures at different locations of the engine and test cell. Pressure data were measured at different locations using Variohm EuroSensor EPT 3100 pressure transducers (max 2 bar). These pressure transducers were calibrated frequently by using a Druck DPI 601 portable pressure indicator/calibrator.

Regulated gaseous emissions were repeatedly measured by a calibrated Horiba MEXA-7100-DEGR exhaust gas analyser directly from the exhaust pipe at different locations. Each measurement is the average of 180 samples (each sample takes 1 s). Horiba MEXA-7100-DEGR uses the chemiluminescence detection (CLD) technique for NO_x and NO, dry non-dispersive Infra-Red (NDIR) technique for CO and CO_2, hot-wet (uncondensed) flame ionisation detector (FID) technique for THC and magneto-pneumatic (MPA) technique to measure oxygen (O_2). Measurement linearity related to using analysers included in the Horiba MEXA-7100-DEGR are all $\leq \pm$ 1% of full-scale output. Engine exhaust gas was delivered to the analyser by means of the heated sampling line with temperature maintained at 191±3°C. The method for derivation of the emission factors from measurements conducted by this instrument is provided in Supplementary Information, section A1.

A calibrated Cambustion DMS500 MKII fast particulate analyser was used to measure exhaust particle size distributions in the size range of approximately 5 nm to 1000 nm. It separates different sizes of particles based on their aerodynamic drag and charge while migrating in an electric field (Cambustion, 2015a). The integrated two-stage dilution system of the utilised DMS500 uses hot compressed air for the first diluter (dilutes at low dilution ratios) and cleaned exhaust gas (by a carbon high-efficiency-particulate-air (HEPA) filter) for the second diluter (dilutes at high dilution ratios using a rotating disk). The first dilution ratio was fixed at 1:5 in the current study. The secondary dilution ratio is normally required to be adjusted to ensure concentrations are within the detectable range. In the current study, the secondary dilution ratio was fixed at approximately 1:100 for the measurements of size distributions before and after the DOC, while for after the DPF measurements, a secondary dilution ratio of 1:1 was used as the particle concentrations were very low. The dilution ratio is calculated automatically using the built-in software and all the results are corrected for the dilution ratio at each test point. Use of a carbon HEPA filter for the secondary diluter, rather than a normal HEPA filter, was designed to strip the majority of the volatile species for the dilution of sampled exhaust gas. A software package utilising a Bayesian statistical algorithm (Cambustion, 2015b) provided by Cambustion was used to separate the nucleation and accumulation modes based on the concentration, mean size and width (geometric standard deviation) of the distribution. In this way, the total concentration of each mode is calculated separately while considering the number of classes per decade of the measurable size range (Cambustion, 2015a). Moreover, total mass can be calculated more accurately, as explained in Cambustion (2015c), since the characteristics (e.g. effective density and physical geometry) of particles of each mode are different. The electrometers of the DMS500 were zeroed before the start of each data point collection using the built-in Autozero function to ensure minimum offset noise effect on the results. The data were averaged over 60 s for a single measurement while each data point presented in this paper is the average of multiple measurements. The standard deviation of the

data was carefully monitored when repeating the experiments to ensure small deviations from the mean value. As an example, the standard deviation of the total particle number concentration was up to 2 orders of magnitude smaller than the mean value of the data points. The method for derivation of the emission factors from measurements performed by the DMS500 is provided in Supplementary Information, section A2. In this paper, the results obtained by using the DMS sampling system are presented in a grey box.

An in-house engine exhaust dilution system (Figure 2) was used for diluting the hot exhaust gas before introducing it to the Nano-Moudi and Particle Size Magnifier systems which are described later in this section. This dilution system incorporates a modified TSI model 3302A diluter. The diluter was modified to use compressed air passed through a high flow rate moisture trap and two HEPA filters. The undiluted hot exhaust sample, delivered *via* a heated line maintained at 191±3°C, mixes with a filtered external airstream at ambient temperature. The sampling lines used in the exhaust dilution and sample collection system are conducting-tubing to minimise any particle loss. Dilution ratio was kept at approximately 1:50±5 confirmed by measurements of NO_x before and after the dilution system. The temperature at the sampling points (after the diluter) was 25±5°C. It should be highlighted that this in-house dilution system is different from the integrated dilution system within the DMS500 (described earlier).

An A10 Particle Size Magnifier (PSM) from Airmodus combined with a TSI 3775 condensation particle counter (CPC) was used to measure particles with mobility diameter between 1.2 nm to 2.5 nm. The PSM grows nanoparticles to the sizes that can be further grown and detected by the CPC (Airmodus, 2017). The condensing liquid used in the PSM was diethylene glycol (Airmodus, 2013) while it was n-butanol in the CPC. The scanning measurement mode of the PSM was used for these experiments which continuously adjusts the cut-off diameter of the PSM (Airmodus, 2013; Kangasluoma et al., 2013). Each sampling event lasted for 30 minutes including 6 scans (each for 5

minutes). The PSM has been calibrated by Airmodus using ammonium sulphate particles produced in a tube furnace and size selected with a high resolution differential mobility analyser (DMA) (Airmodus, 2013). The method for derivation of the emission factors from measurements done by the PSM system is provided in Supplementary Information, section A3.

A Nano-micro orifice uniform deposit impactor (Nano-Moudi) 125 instrument from MSP Copley Scientific was utilised for collecting exhaust particles at different sizes for size-resolved characterisation of the I+SVOC. In a Nano-Moudi (an inertial impactor), particles are collected on different stages based on the Stokes number which is a function of particle density, slip correction, particle diameter, air viscosity, nozzle diameter and volumetric flow rate through the nozzle. Thirteen stages of the Nano-Moudi from S1 to S13 with nominal 50% cut-points of 10000, 5600, 3200, 1800, 1000, 560, 320, 180, 100, 56, 32, 18 and 10 nm, respectively, were used in this study. In this paper, when discussing Nano-Moudi results of >100 nm, for example, it means particles in the diameter range of 100 nm to 180 nm (the cut-point of the previous stage); this does not apply to S1 as there is no stage before it. Volumetric flow rate through the Nano-Moudi was 9 litres per minute and samples were collected for 30 minutes using polypropylene backed PTFE 47 mm filters from Whatman.

I+SVOC on each stage of the Nano-Moudi were characterised using two-dimensional gas chromatography time-of-flight mass spectrometry (GC×GC-ToF-MS). Details of this GC×GC-ToF-MS characterisation method are provided by Alam et al. (2019). Briefly, the PTFE filters were spiked with internal standards and subsequently were immersed in dichloromethane (DCM) and then the mixture was ultrasonicated for 20 minutes at 20°C. The extract was concentrated to 50 µL under a gentle flow of nitrogen. Then this sample was analysed by means of a two-column GC 7890A from Agilent Technologies equipped with a cryogenic modulator (Zoex ZX2). The GC×GC was connected to a Bench-ToF-Select from Markes International. The scan speed and ionisation

energy were set at 50 Hz and 70 eV, respectively. Details of the temperature ramp settings are provided by Alam et al. (2016). All the analysis include consideration of internal standards and subtraction of the I+SVOC content found on the blank filters. Solvent blank injections and blank filter extractions both did not show any peaks in the chromatography and so all compounds are below the detection limit, indicating no instrument artefacts (please refer to Alam et al. (2019) for more information). Data were processed and post-processed *via* GC Image v2.5 from Zoex Corporation. Computer language for identifying chemical (CLIC) was used to characterise different classes of I+SVOC within each sample. Using this technique in earlier work (Alam et al., 2018), we reported mass closures of approximately 90% and 75% for diesel fuel and engine lubricating oil samples and around 85% and 75% of the total ion current were identified for gas and particle phase diesel engine I+SVOC emissions respectively. The uncertainty of this analysis method is approximately 24% and more details are provided in Alam et al. (2108). Repeatability of the I+SVOC volatility profile and concentration has been ensured during different testing campaigns and also by comparing Nano-Moudi results with those of single PTFE filters using the same engine but at different times. In the current study, we found that C_{13} to C_{37} alkanes (including straight- and branched-chain), C_{14} to C_{32} cycloalkanes, C_{16} to C_{23} bicyclic alkanes, C_{13} to C_{26} monocyclic aromatics and C_9 to C_{27} oxygenated compounds (including ketones, aldehydes and furanones) are the most abundant I+SVOC classes in the diesel exhaust particle samples and therefore are the focus of this paper. The method for derivation of the I+SVOC emission factors is provided in Supplementary Information, section A4.

3. RESULTS AND DISCUSSION

3.1 Regulated Gaseous Emissions and Particle Size Distribution

3.1.1 Gaseous emissions

Gaseous emission factors and their reduction percentage (conversion or reduction efficiency depending on the species) over the aftertreatment devices are listed in Table 2. Engine-out (before

DOC) emission factors for CO and THC at this low load engine condition were relatively high because of lower combustion efficiency. However, their conversion efficiencies were high and they were decreased at two separate stages – once over the DOC and once over the DPF. This is an indication that the utilised DPF is catalyst coated. In addition, these results confirm that the DOC and DPF were in an active state for converting HC, which is important for discussing I+SVOC results later in this section. It is believed that the absence of NO_2 production was due to the fact that the operating temperature was not high enough (was below 200°C) to initiate this process (Kim et al., 2011). The conversion of NO_2 to NO is believed to be due to its decomposition and consumption of its oxygen content by the available CO and HC on the catalyst active sites. There was an overall reduction of NO_x due to conversion of NO to N_2 over the catalysts. Exhaust gas temperature after the DOC, before entering the DPF, increased by approximately 23°C and this is believed to be because of exothermic reactions within the DOC (e.g. combustion of CO and HC which subsequently increased the CO_2 concentration).

3.1.2 Particle emissions

Effects of the DOC and DPF on the size distribution of particle emissions can be seen in Figure 3. In this figure, particles with diameter between 1.2 and 2.5 nm were measured by the PSM system and particles with diameter between 4.87 and 1000 nm were measured by the DMS system (refer to the experimental setup section). Volume size distributions (Figure 3 (b)) were calculated under the assumption that all particles have a completely spherical geometry – an assumption that may not be completely correct for larger diesel exhaust particles, especially in the accumulation mode (Kittelson, 1998).

PSM results showed a high concentration peak at approximately 1.5 nm in the samples taken both before and after the DOC (Figure 3 (a)). The concentration was the highest for measurements before the DOC, decreased after the DOC, and was negligible after the DOC+DPF. The possibility of

formation and/or growth of small particles in the exhaust dilution system is reduced when concentrations of gaseous volatile and semi-volatile HC are decreased by using a DOC. For such small particles, kinetic limitations to the loss of semi-volatile constituents are very small, and therefore even constituents of quite low volatility can evaporate. Considering the results before and after the DOC+DPF system, one can conclude that the sub-2.5 nm particle emissions from the current diesel engine contain both volatile and non-volatile constituents. The non-volatile nuclei are efficiently removed by the DPF as shown in Figure 3 as also reported by Filippo and Maricq (2008) for light-duty diesel vehicles. The sources of these particles (which presumably include a solid core) are assumed to be in high temperature regions inside or in the vicinity of the combustion chamber due to their electrical charge (Filippo and Maricq, 2008; Alanen et al., 2015; Sgro et al., 2012). Sulphur storage and release in the newly-fitted aftertreatment system (acting as a reservoir) is another possibility (Herner et al., 2011; Kittelson et al., 2006). It has been reported that sulphur storage and release mechanisms are more related to the DOC rather than the DPF of the aftertreatment system (Swanson et al., 2009). Within a DOC or a catalysed DPF, engine out SO_2 can convert to SO_3. SO_3 can react with H_2O and form H_2SO_4 (sulphuric acid) which can nucleate under the atmospheric conditions. Tiszenkel et al. (2019) conducted a preliminary study about the effects of temperature on the nucleation and growth of sulphuric acid using the Tandem Aerosol Nucleation and Growth Environment Tube (TANGENT). They used a PSM after the nucleation tube of the TANGENT system and confirmed that at temperatures around 24°C, similar to the temperature of the dilution point for the PSM results in the current study, clusters with a diameter of 1.65-1.70 nm were formed, hypothetically via a ternary process. This diameter, which is close to the peak concentration diameters measured in the current study, did not change significantly as the sulphuric acid concentration was increased. This finding can indicate a possible role of sulphuric acid in forming sub-2.5 nm particles, although the exhaust gas mixture is very different to the mixture that Tiszenkel et al. (2019) studied. However, in the current study, the sulphur content of the ULSD fuel was very low (approximately 8 mg/kg), but the sulphur content of the engine

lubricating oil and its contribution to the emissions are unknown. It would be interesting to investigate the sensitivity of size distribution and characteristics of these very small diesel exhaust particles to the dilution conditions, e.g. dilution ratio and relative humidity as two important factors (Shi and Harrison, 1999).

Bimodal particle size distributions, with both modes of nucleation and accumulation (the latter also referred to as the soot mode), were detected in measurements by the DMS upstream and downstream of the DOC (Figure 3(a)). Particle concentrations after the DPF appear to be negligible – there was no sign of an enhanced nucleation mode concentration which has been reported by other researchers for some engine operating conditions (Herner et al., 2011). Count median diameter (CMD) of the nucleation mode particles was 19.3 and 17.6 nm upstream and downstream of the DOC, respectively. CMD of accumulation mode particles upstream and downstream of the DOC was 54.9 and 50.4 nm, respectively.

The DOC had a considerable effect in reducing the nucleation mode particles – mass decreased from 0.0094 to 0.0032 g/kg$_f$. The nucleation mode comprises particles with a small non-volatile core (ca 5 nm) and a major part condensed semi-volatile HC (Filippo and Maricq, 2008; Lähde et al., 2009; Rönkkö et al., 2007). In the dilution system and in the presence of soot particles, semi-volatile HC, which can also nucleate during dilution, can be adsorbed by the soot surface and increase the size and mass of particle emissions. The DOC oxidises some of the gaseous HC and therefore contributes to a reduction in nucleation mode particle number.

There was also a reduction of the accumulation mode particles in the DOC – mass decreased from 0.2063 to 0.1664 g/kg$_f$. The accumulation mode comprises a larger graphitic carbon core, with a coating of condensed semi-volatile HC (Shi et al., 1999; Shi et al., 2000). Exothermic reactions inside the DOC can increase the temperature near active sites and may facilitate oxidation of HC

already adsorbed on soot particles. However, the data in Figure 3 show little change in particle size on passing through the DOC. These particles can also deposit on the top and to the monolith walls of the DOC (Eastwood, 2008). These deposited particles cannot be catalytically converted and therefore may only be oxidised under high temperature conditions. Therefore, the results suggests both loss of particles in the DOC and particle shrinkage due to HC oxidation.

Figure 3(b) illustrates that the peak of volume size distribution was associated with particles with diameter of 100 nm for measurements before the DOC. The majority of volume (and presumably mass) of particles are present around this particle diameter. Particles measured by the PSM made very little contribution to the total volume due to their small diameter.

3.2 Particle Phase I+SVOC Composition and Size Distribution

Table 3 shows the results for particle mass (using the DMS) and I+SVOC mass (using the Nano-Moudi). In this table, nucleation mode (Nuc.) particle mass and accumulation mode (Acc.) particle mass (calculated as described in the experimental setup section) were added to calculate the total particle mass (PM). The DMS results after the DOC+DPF showed a very small number of particles and therefore no peaks of nucleation and accumulation were detected using the log-normalisation method. Total mass of each I+SVOC class (namely alkanes, cycloalkanes, bicyclic alkanes, monocyclic aromatics and oxygenated compounds) were calculated by adding the data of Nano-Moudi stages below 1000 nm, which is the maximum measurable diameter by the utilised DMS. This was done in order to help elucidate the relation between total PM and total I+SVOC (addition of all classes) and each I+SVOC class.

Total PM decreased by approximately 21%, comparing measurements before and after the DOC and this was driven by the decrease of both nucleation and accumulation mode particles. Total particle phase I+SVOC before the DOC made a high contribution to the total PM (more than 48%) as presented in Table 4. Similar to the observations for gas phase THC that were discussed earlier,

particle phase I+SVOC concentrations decreased in two stages, once over the DOC and once over the DPF. The reduction percentage of total particle phase I+SVOC over the DOC was more than 74% and over the DOC+DPF was approximately 91%. The DOC can help oxidise the engine-out gas phase SVOC (Liu et al., 2018) and consequently decrease the particle phase I+SVOC collected in the diluted exhaust. Later, when the exhaust gas passes the catalysed DPF, apart from further conversion of I+SVOC, particles are physically trapped. After the DPF, the number of solid core particles is low and consequently less condensation sink is available for the gas phase I+SVOC (if any) to condense/adsorb on them. In the current study, the particle phase I+SVOC measured after the DOC+DPF must have mainly derived from vapour passing the DOC and DPF which condensed on the filters after the dilution, as the DMS showed negligible measureable particles exiting the DPF. It should be borne in mind that the DMS and Nano-Moudi used different dilution systems (described in the experimental setup section) while the conditions of the Nano-Moudi dilution system were more similar to the atmospheric dilution (dilution with only ambient air). Moreover, the utilised comprehensive GC technique has a high sensitivity for measuring small concentrations (a few ng/m^3) of I+SVOC. Although adsorption artefacts are not expected to be very high on the PTFE filters used in this study, a small amount of gas phase I+SVOC condensation and adsorption on stages of the Nano-Moudi at different sampling locations could have happened. Further to the current study, it would be interesting to investigate the effects of varying the dilution conditions such as dilution ratio, temperature, pressure and relative humidity on the concentrations and characteristics of different I+SVOC classes in different particle size ranges.

Total particle phase I+SVOC mass after the DOC+DPF was approximately 8.9 mg/kg_f. Gordon et al. (2014) conducted an environmental chamber study and reported emission factors of <~10 mg/kg_f for total black-carbon and POA and SOA for medium/heavy-duty diesel vehicles equipped with a catalysed DPF. Although PTFE filters were used for the current study and adsorption artefacts are not expected to be so severe, it may be worthy of mention that May et al. (2013) reported that for

the test vehicles equipped with a DPF, up to 90% of the POA collected on the quartz filters from the constant volume sampler were actually adsorbed vapours. It is expected that comprehensive analysis of gas phase I+SVOC after the DPF will clarify gas-particle partitioning under various dilution conditions.

Among the different I+SVOC classes, alkanes had the highest mass ratio to the total measured PM (Table 4) and I+SVOC (Table 5) at each sampling location. This was expected since the results from earlier analyses of diesel fuel and engine lubricating oil indicated the abundance of alkanes (Funkenbusch et al., 1979; Alam et al., 2016; Zeraati-Rezaei et al., 2016; Alam et al., 2018; Liang et al., 2018). The I+SVOC content found in the particle phase is very similar to that found in the engine lubricating oil (Zeraati-Rezaei et al., 2016; Alam et al., 2018). Alkanes and monocyclic aromatics had the highest conversion efficiency (decrease percentage or removal efficiency) over the DOC and the lowest was for oxygenated compounds (Table 3). These results highlight the lower catalytic reactivity for the cyclic alkanes compared to total normal- and branched-alkanes. Semi-volatile oxygenated compounds, which are believed to be products of combustion of fuel and lubricating oil within the engine, decreased by only ~20% over the DOC and therefore made a higher contribution to the total PM and I+SVOC after the DOC. This can be due to the partial oxidation and breakdown of different compounds over the DOC and their appearance as oxygenated compounds – further discussion is provided later in this section. Generally, the decrease in concentration of all I+SVOC classes was more than 90% over the DOC+DPF except for oxygenated compounds which was approximately 76%. Since the utilised DPF was catalysed, it can be hypothesised that the oxidation process of the gas phase I+SVOC in the DPF was ongoing during the sampling. This process can result in gas phase partial oxidation by-products that can condense/adsorb on the existing particles or the PTFE filter.

For a more detailed analysis, Figure 4 (a, b, c) illustrates emission factors for different classes of I+SVOC (total alkanes, cycloalkanes, bicyclic alkanes (bicyclics), monocyclic aromatics (monoaromatics) and oxygenated compounds (oxygenates) in different size bins (sampled using the Nano-Moudi) before DOC, after DOC and after DOC+DPF. This figure also includes the conversion efficiency of each class of I+SVOC at each size bin (stage) when using the DOC (Figure 4(b)) and DOC+DPF (Figure 4(c)). Contour plots showing particle size and carbon number for each I+SVOC class and measurement location are available in Figure 5 and Supplementary Information, sections C1 to C4. Tables of the raw data ($\mu g/kg_f$) containing size bin and carbon number for each class and measurement location can be found in Supplementary Information, sections B1 to B5.

The peak concentration of total I+SVOC upstream of the DOC was found in the size bin close to 100 nm. This is probably due to the higher total mass of particles in this size range – the peak of particle volume shown in Figure 3(b) was at the same particle diameter. This may also indicate that although particles in the accumulation mode are formed of both carbonaceous cores and I+SVOC coatings, their I+SVOC fraction upstream of the DOC is high at this engine condition. Moreover, in the dilution system, due to their high concentration and total surface area, they act as sinks for the available gas phase I+SVOC to condense/adsorb on. It may be worthy of mention that I+SVOC concentration in the size bins >5600 and >10000 nm are relatively high. In the current study, measurement of size distribution for these large particles was not available; however, it is hypothesised that even if their concentrations have been low they could act as sinks for the gas phase I+SVOC as they have large surface areas and are collected on the two top stages in the Nano-Moudi.

Alkanes were generally the dominant mass fraction in each size bin at the three measurement locations. In terms of conversion efficiency when using the DOC, they generally had the highest values across different stages followed closely by monoaromatics and then bicyclics>cycloalkanes.

Oxygenated compounds had the lowest conversion efficiency, if this is a correct interpretation. For oxygenated compounds, as shown in Figure 4 and Supplementary Information, section C4, except for size bins >3200 nm, the size distribution of I+SVOC did not change considerably (reduction percentage was ~20% for all). Therefore, if there were gas phase I+SVOC partial oxidation processes, the by-products were evenly condensed/adsorbed on different particle size bins after the DOC. Conversion efficiency of different classes in the size range of 10 to 18 nm (S13) was relatively low. It should be noted that the concentration of I+SVOC before the DOC was the lowest in this size bin. Due to the small physical size of these particles, their high surface to volume ratio can cause them to adsorb more vapour. When the DPF was added to the system, conversion efficiency of all classes (except oxygenated compounds) in all size ranges was more than approximately 85%.

Figure 6 illustrates the concentration of different I+SVOC classes based on the carbon number. The presented data is the sum of concentrations available in all of the size bins of the Nano-Moudi. In the results upstream of the DOC, a bimodal distribution of alkanes, based on the carbon number, was found in the particle phase diesel I+SVOC emissions; this has been also reported by Black and High (1979) and Alam et al. (2016). Diesel fuel and engine lubricating oil are the sources of these two peaks; the first peak is from lighter HC in the fuel and the second peak is from heavier HC in the oil.

Similar to the observations when analysing various lubricating oil samples (Funkenbusch et al., 1979; Zeraati-Rezaei et al., 2016; Alam et al., 2018; Liang et al., 2018), alkanes with carbon number around 24 had the highest contribution to the total amount of I+SVOC collected in the current experiments. C_{20} had the highest concentration for the oxygenated compounds and C_{22} had the highest concentration for the rest of the analysed I+SVOC classes.

The efficiency of the DOC in removing I+SVOC depended on both the class of compounds and carbon number. In the case of alkanes, conversion efficiency of C_{20} to C_{34} was a little lower than the rest of the analysed range. Oxidation theory cannot always explain the experimental data, suggesting that there may be other removal mechanisms (Majewski and Khair, 2006). In theory, once the catalyst reaches the light-off temperature for a specific exhaust constituent, the rate of oxidation is controlled by the rate of mass transfer or diffusion rate of that species. This implies that there is more diffusion of low molecular weight HC with higher volatility compared to high molecular weight HC. However, short chain alkanes are known to have higher light-off temperatures compared to longer chain alkanes. As opposed to theory, interestingly, some studies have shown that longer chain HC were removed more efficiently over a catalyst (Eastwood, 2008; Johnson and Kittelson, 1994). Research shows that decreasing C-H bond strength of n-alkanes with increasing their chain length reduces their surface ignition temperature on a catalyst (Veser et al., 1999; Hunter and East, 2002; Diehl et al., 2010), and hence longer chain n-alkanes are more reactive over a catalyst. In addition, this behaviour of the DOC might be partly explained by the fact that there are possibilities that heavier HC can be catalytically cracked into lighter HC (Majewski and Khair, 2006).

Generally, conversion efficiency of semi-volatile cycloalkanes with higher carbon number was less than the ones with lower carbon number over the DOC. The trend for bicyclic alkanes was similar to the trend for alkanes – higher at the beginning and end of the carbon number range, while C_{18} and C_{19} bicyclic alkanes had low conversion efficiencies (<35%). Conversion efficiency of monocyclic aromatics with carbon number ≥18 was high (Figure 6). Conversion efficiency of oxygenated compounds with 9≤carbon number≤17 was generally less than 10%. It can be hypothesised that these relatively lighter I+SVOC that appeared after the DOC were by-products of synthesis from partial oxidation of heavier I+SVOC.

603 Using the DOC+DPF, reduction percentage of all the classes (except oxygenated compounds) was
604 generally more than 80% for different carbon numbers with the possible exception of low
605 concentration C_{13} and C_{14} monocyclic aromatics, although this looks likely to be an artefact of
606 imprecision of the very low concentrations measured.
607
608 **4. SUMMARY AND CONCLUSIONS**
609 Size-resolved physico-chemical characteristics of the intermediate- and semi-volatile particle
610 emissions from a light-duty diesel engine have been investigated upstream and downstream of the
611 diesel oxidation catalyst (DOC) and the catalysed diesel particulate filter (DPF). Particle phase
612 intermediate- and semi-volatile organic compounds (I+SVOC) have been comprehensively
613 characterised based on the compound type (class) and carbon number using a multi-stage Nano
614 impactor and GC×GC-ToF-MS technique. The number size distributions of particles between 1.2-
615 1000 nm have been also investigated. The DOC and the DPF were in an active state for converting
616 hydrocarbons.
617 In samples taken before the DOC, the emission factor for total I+SVOC found in the sub-1000 nm
618 particles was 104.8 mg/kg_f. I+SVOC made a large contribution to the total mass of particles
619 (~49%), and alkanes had the highest mass ratio to the total I+SVOC (~63%). The concentrations of
620 different classes of I+SVOC emissions were ranked as alkanes (65.6 mg/kg_f) >cycloalkanes
621 >monoaromatics =oxygenates >bicyclics (8.2 mg/kg_f). As a summary, Figure 5 shows the
622 concentration of alkanes (the most abundant class similar to the observations in the lubricating oil
623 analysis) with respect to the carbon number and particle diameter. Importantly, before the DOC, the
624 peak concentration of all classes was found in the particle size bin close to 100 nm due to the higher
625 total mass of particles in this size bin. This is indicative of a high concentration of I+SVOC
626 constituents in the accumulation mode particle emissions from the light-duty engine. Before the
627 DOC, alkanes with carbon number around 24 made the largest contribution to the total I+SVOC

628 mass, while C_{22} had the highest concentration for cycloalkanes, bicyclics and monoaromatics, and it
629 was C_{20} for the oxygenates.
630 Similar to the gaseous total hydrocarbons, particle phase total I+SVOC emissions decreased in two
631 stages, firstly over the DOC (by ~75%) and then over the DPF (total ~92%). After the DOC, total
632 I+SVOC made a smaller contribution to the total particle mass (~16%). The removal efficiency of
633 different I+SVOC species over the DOC was ranked as monoaromatics (~85%) >alkanes >bicyclics
634 >cycloalkanes >oxygenates (~20%). Using the DOC+DPF system resulted in removal efficiencies
635 of >90% for all classes of I+SVOC except oxygenates which was approximately 76%. Due to the
636 lower removal efficiency of the oxygenates, their concentrations were the highest after alkanes in
637 the measurements after the DOC and DOC+DPF. This was presumably due to the ongoing
638 oxidation of various species inside the DOC and DPF. Some of the lighter I+SVOC that were
639 measured after the aftertreatment devices are believed to be by-products of synthesis and partial
640 oxidation of heavier I+SVOC. Generally, I+SVOC found in the particle size range of 10 nm to 18
641 nm had the lowest removal efficiencies over the DOC probably due to their higher surface to
642 volume ratio which makes them susceptible to adsorb more vapour. With the addition of the DPF,
643 in general, I+SVOC were evenly removed from different particle size bins.
644 High concentrations of sub-2.5 nm particles were measured and the peak was approximately
645 1.9×10^{15} particles/kg_f (dN/dlogdp/kg_f) at around 1.5 nm. This peak decreased by >50% after the
646 DOC and was much lower (1.1×10^{14} parts/kg_f) after the DOC+DPF. These reductions are believed
647 to be due to both the loss of intermediate- and semi-volatile constituents and physical filtration. It is
648 hypothesised that these particles have both volatile and non-volatile constituents.
649
650 The results of this study can be used as an input and validation database for various modelling
651 platforms considering source emissions at low engine loads. In future studies, it is suggested that
652 size-resolved characteristics of I+SVOC and sub-2.5nm particles emissions are investigated under
653 various engine loads and speeds as well as transient engine conditions, and consequently various

gas hourly space velocities for the oxidation catalysts and filters as well as active regeneration of the filters. These complementary investigations can eventually help interpret the real driving emissions (RDE) when the engine and aftertreatment systems undergo various operating modes.

DATA ACCESSIBILITY

Data supporting this publication are openly available from the UBIRA eData repository at https://doi.org/10.25500/edata.bham.00000339.

ACKNOWLEDGMENTS

This work is a part of the FASTER project (ERC-2012-AdG, proposal no. 320821) sponsored by the European Research Council (ERC). The work was partially supported by the Natural Environment Research Council through its support of the National Centre for Atmospheric Science (grant number R8/H12/83/011). The authors would like to thank Yasser Al Qahtani and Zhirong Liang for their contribution during engine experiments and Chris Stark for his contribution in GC analysis.

671 **REFERENCES**

672 Airmodus, 2017. A10 Particle Size Magnifier. Available from: http://www.airmodus.com/a10/
673 [Accessed 25/01/2017].
674
675 Airmodus, 2013. Particle Size Magnifier Model A10 User Manual A13TD0012, A13TD0012 ed.
676
677 Alam, M. S., Zeraati-Rezaei, S., Stark, C. P., Liang, Z., Xu, H. and Harrison, R. M., 2016. The
678 characterisation of diesel exhaust particles-composition, size distribution and partitioning, Faraday
679 Discuss., 189, 69-84.
680
681 Alam, M. S., Zeraati-Rezaei, S., Liang, Z., Stark, C., Xu, H., MacKenzie, A. R. and Harrison R. M.,
682 2018. Mapping and quantifying isomer sets of hydrocarbons (≥ C12) in diesel exhaust, lubricating
683 oil and diesel fuel samples using GC × GC-ToF-MS, Atmos. Measure. Techn., 11, 3047-58.
684
685 Alam, M. S., Zeraati-Rezaei, S., Xu, H. and Harrison, R. M., 2019. Characterisation of Gas and
686 Particulate Phase Organic Emissions (C_9-C_{37}) from a Diesel Engine and the Effect of Abatement
687 Devices, Environ. Sci. Technol., Environ. Sci. Technol., 53, 11345-11352.
688
689 Alanen, J., Saukko, E., Lehtoranta, K., Murtonen, T., Timonen, H., Hillamo, R., Karjalainen, P.,
690 Kuuluvainen, H., Harra, J., Keskinen, J., Rönkkö, T., 2015. The formation and physical properties
691 of the particle emissions from a natural gas engine, Fuel, 162, 155-161.
692
693 Black, F. and High, L., 1979. Methodology for determining particulate and gaseous diesel
694 hydrocarbon emissions, SAE Intl., SAE Techn. Paper 790422, https://doi.org/10.4271/790422.
695
696 Cambustion, 2015(a). DMS500 Fast Particulate Analyzer - User Manual - Version 4.03.
697
698 Cambustion, 2015(b). Cambustion Application Note DMS06 - Real-time Mode Finding &
699 Lognormal Fitting with DMS Series Fast Particulate Spectrometers. Available from:
700 http://www.cambustion.com/sites/default/files/applications/DMS/dms06v03.pdf [Accessed
701 16/02/2017 2017].
702
703 Cambustion, 2015(c). Cambustion Application Note DMS01 - Particulate Mass Measurement with
704 DMS Series Fast Spectrometers. Available from:
705 http://www.cambustion.com/sites/default/files/applications/DMS/dms01v05.pdf [Accessed
706 30/07/2016 2016].
707
708 Charron, A. and Harrison, R.M., 2003. Primary particle formation from vehicle emissions during
709 exhaust dilution in the roadside atmosphere, Atmos. Environ., 37, 4109-4119.
710
711 Dall'Osto, M., Thorpe, A., Beddows, D.C. S., Harrison, R. M., Barlow, J. F., Dunbar, T., Williams,
712 P. I. and Coe, H., 2011. Remarkable dynamics of nanoparticles in the urban atmosphere, Atmos.
713 Chem. Phys., 11, 6623-6637.
714
715 Department-for-Transport-UK, 2018. Vehicle Licensing Statistics: Quarter 2 (Apr – Jun 2018).
716 Available from:
717 https://assets.publishing.service.gov.uk/government/uploads/system/uploads/attachment_data/file/7
718 40109/vehicle-licensing-statistics-april-to-june-2018.pdf [Accessed 09/02/2019 2019].
719

Diehl, F., Barbier Jr, J., Duprez, D., Guibard, I. and Mabilon, G., 2010. Catalytic oxidation of heavy hydrocarbons over Pt/Al2O3, Influence of the structure of the molecule on its reactivity, Appl. Catal. B-Environ., 95, 217-27.

Donahue, N. M., Robinson, A. L., Stanier, C. O. and Pandis, S. N., 2006. Coupled partitioning, dilution, and chemical aging of semivolatile organics, Environ. Sci. Technol., 40, 2635-43.

Drozd, G. T., Zhao, Y., Saliba, G., Frodin, B., Maddox, C., Oliver Chang, M.-C., Maldonado, H., Sardar, S., Weber, R. J., Robinson, A. L. and Goldstein, A. H., 2019. Detailed speciation of intermediate volatility and semivolatile organic compound emissions from gasoline vehicles: Effects of cold-starts and implications for secondary organic aerosol formation, Environ. Sci. Technol., 53, 1706-14.

Eastwood P., 2008. Particulate Emissions from Vehicles, SAE International and Wiley-PEPublishing Series.

Filippo, A. D. and Maricq M. M., 2008. Diesel nucleation mode particles: semivolatile or solid?, Environ, Sci,Technol., 42, 7957-7962.

Funkenbusch, E. F., Leddy, D. G. and Johnson J. H., 1979. The characterization of the soluble organic fraction of diesel particulate matter, SAE Intl., SAE Techn. Paper 790418, https://doi.org/10.4271/790418.

Gordon, T. D., Presto, A. A., Nguyen, N. T., Robertson, W. H., Na, K., Sahay, K. N., Zhang, M., Maddox, C., Rieger, P., Chattopadhyay, S., Maldonado, H., Maricq, M. M. and Robinson, A. L., 2014. Secondary organic aerosol production from diesel vehicle exhaust: impact of aftertreatment, fuel chemistry and driving cycle, Atmos. Chem. Phys., 14, 4643-59.

Herner, J. D., Hu, S., Robertson, W. H., Huai, T., Chang, M. C. O., Rieger, P. and Ayala. A., 2011. Effect of advanced aftertreatment for PM and NOx reduction on heavy-duty diesel engine ultrafine particle emissions, Environ. Sci.Technol., 45, 2413-9.

Heywood, J. B., 1988. Internal Combustion Engine Fundamentals, McGraw-Hill.

Hietikko, R., Kuuluvainen, H., Harrison, R.M., Portin, H., Timonen, H., Niemi, J.V. and Rönkkö T., 2018. Diurnal variation of nanocluster aerosol concentrations and emission factors in a street canyon, Atmos. Environ., 189, 98-106.

Huang, L., Bohac, S. V., Chernyak, S. M. and Batterman, S. A., 2015. Effects of fuels, engine load and exhaust after-treatment on diesel engine SVOC emissions and development of SVOC profiles for receptor modeling, Atmos. Environ. 1994, 102, 229-38.

Hunter, K. C. and East, A. L. L., 2002. Properties of C−C bonds in n-alkanes: Relevance to cracking mechanisms, J. Phys. Chem. A, 106, 1346-56.

IEA, 2016. Energy and Air Pollution. Available from: http://www.iea.org/publications/freepublications/publication/WorldEnergyOutlookSpecialReport2016EnergyandAirPollution.pdf [Accessed 01/07/2016 2016].

ICCT, 2018. European Vehicle Market Statistics, Pocketbook 2018/19. Available from: https://www.theicct.org/sites/default/files/publications/ICCT_Pocketbook_2018_Final_20181205.pdf [Accessed 09/02/2019 2019].

771 Järvinen, A., H. Timonen, P. Karjalainen, M. Bloss, P. Simonen, S. Saarikoski, H. Kuuluvainen, J.
772 Kalliokoski, M. Dal Maso, J. V. Niemi, J. Keskinen and T. Rönkkö, 2019. Particle emissions of
773 Euro VI, EEV and retrofitted EEV city buses in real traffic, Environ. Pollut., 250: 708-716.
774
775 Johnson, J. E. and Kittelson, D. B., 1994. Physical factors affecting hydrocarbon oxidation in a
776 diesel oxidation catalyst, SAE Intl., SAE Technical Paper 941771, https://doi.org/10.4271/941771.
777
778 Kangasluoma, J., Junninen, H., Lehtipalo, K., Mikkilä, J., Vanhanen, J., Attoui, M., Sipila, M.,
779 Worsnop, D., Kulmala, M. and Petaja, T., 2013. Remarks on ion generation for cpc detection
780 efficiency studies in sub-3-nm size range, Aerosol Sci. Technol., 47, 556-63.
781
782 Kim, C. H., Schmid, M., Schmieg, S. J., Tan, J. and Li, W., 2011. The effect of Pt-Pd ratio on
783 oxidation catalysts under simulated diesel exhaust, SAE Intl., SAE Technical Paper 2011-01-1134,
784 https://doi.org/10.4271/2011-01-1134.
785
786 Kittelson D. B., 1998. Engines and nanoparticles: a review, J. Aerosol Sci., 29, 575-88.
787
788 Kittelson, D. B., Watts, W. F., Johnson, J. P., Rowntree, C., Payne, M., Goodier, S., Warrens, C.,
789 Preston, H., Zink, U., Ortiz, M., Goersmann, C., Twigg, M. V., Walker ,A. P. and Caldow R., 2006.
790 On-road evaluation of two diesel exhaust aftertreatment devices, J. Aerosol Sci., 37, 1140-51.
791
792 Lähde, T., Rönkkö, T., Virtanen, A., Schuck, T. J., Pirjola, L., Hämeri, K., Kulmala, M., Arnold, F.,
793 Rothe, D. and J. Keskinen, 2009. Heavy duty diesel engine exhaust aerosol particle and ion
794 measurements, Environ. Sci. Technol., 43, 163-8.
795
796 Laurence, R. B., Wong, V. W., Brown, A. J., 1996. Effects of lubrication system parameters on
797 diesel particulate emission characteristics, SAE Intl., SAE Techn. Paper 960318,
798 https://doi.org/10.4271/960318.
799
800 Liang, Z., Alam, M. S., Zeraati Rezaei, S., Stark, C., Xu, H. and Harrison, R. M., 2018.
801 Comprehensive chemical characterization of lubricating oils used in modern vehicular engines
802 utilizing GC × GC-TOFMS, Fuel, 220, 792-799.
803
804 Liu, Z. G., Eckerle, W. A. and Ottinger, N. A., 2018. Gas-phase and semivolatile organic emissions
805 from a modern nonroad diesel engine equipped with advanced aftertreatment, JAWMA, 68, 1333-
806 45.
807
808 Majewski, W. A. and Khair, M. K., 2006. Diesel emissions and their control, 584pp, SAE Intl.,
809 ISBN 10: 0768006740 ISBN 13: 9780768006742.
810
811 May, A. A., Presto, A. A., Hennigan, C. J., Nguyen, N. T., Gordon, T. D. and Robinson, A. L.,
812 2013. Gas-particle partitioning of primary organic aerosol emissions: (2) diesel vehicles, Environ.
813 Sci. Technol., 47, 8288-96.
814
815 Nikolova, I., Cai, X., Alam, M. S., Zeraati-Rezaei, S., Zhong, J., MacKenzie, A. R. and Harrison, R.
816 M., 2018. The influence of particle composition upon the evolution of urban ultrafine diesel
817 particles on the neighbourhood scale, Atmos. Chem. Phys., 18, 17143-55.
818
819 Robinson, A. L., Donahue, N. M., Shrivastava, M. K., Weitkamp, E. A., Sage, A. M., Grieshop A.
820 P., Lane, T. E., Pierce, J. R., Pandis, S. N., 2007. Rethinking organic aerosols: Semivolatile
821 emissions and photochemical aging, Science, 315, 1259.
822

Rönkkö, T., Virtanen, A., Kannosto, J., Keskinen, J., Lappi, M. and Pirjola, L., 2007. Nucleation mode particles with a nonvolatile core in the exhaust of a heavy duty diesel vehicle, Environ. Sci. Technol., 41, 6384-9.

Rönkkö, T., H. Kuuluvainen, P. Karjalainen, J. Keskinen, R. Hillamo, J. V. Niemi, L. Pirjola, H. J. Timonen, S. Saarikoski, E. Saukko, A. Järvinen, H. Silvennoinen, A. Rostedt, M. Olin, J. Yli-Ojanperä, P. Nousiainen, A. Kousa and M. Dal Maso, 2017. Traffic is a major source of atmospheric nanocluster aerosol., Proceedings of the National Academy of Sciences 114(29): 7549.

Sakurai, H., Tobias, H. J., Park, K., Zarling, D., Docherty, K. S., Kittelson, D. B., McMurry, P. H., Ziemann, P. J., 2003. On-line measurements of diesel nanoparticle composition and volatility, Atmos. Environ., 37, 1199-210.

Sgro, L. A., Sementa, P., Vaglieco, B. M., Rusciano, G., D'Anna, A.and Minutolo, P., 2012. Investigating the origin of nuclei particles in GDI engine exhausts, Combust. Flame, 159, 1687-1692.

Shi, J. P. and Harrison, R. M., 1999. Investigation of ultrafine particle formation during diesel exhaust dilution, Environ. Sci.Technol., 33, 3730-3736.

Shi, J. P., Mark, D. and Harrison, R. M., 2000. Characterization of particles from a current technology heavy-duty diesel engine, Environ. Sci.Technol., 34, 748-55.

Stone, R., 1999. Introduction to Internal Combustion Engines. Third ed., MacMillan Press Ltd.

Swanson, J. J., Kittelson, D. B., Watts, W. F., Gladis, D. D. and Twigg, M. V., 2009. Influence of storage and release on particle emissions from new and used CRTs, Atmos. Environ., 43, 3998-4004.

Tiszenkel, L., C. Stangl, J. Krasnomowitz, Q. Ouyang, H. Yu, M. J. Apsokardu, M. V. Johnston and S.-H. Lee, 2019. Temperature effects on sulfuric acid aerosol nucleation and growth: initial results from the TANGENT study. Atmos. Chem. Phys, 19(13): 8915-8929.

Veser, G., Ziauddin, M. and Schmidt, L. D., 1999. Ignition in alkane oxidation on noble-metal catalysts, Catalysis Today, 47, 219-28.

Zeraati-Rezaei, S., Alam, M. S., Liang, Z., Stark, C. P., Harrison, R. M. and Xu, H., 2016. Investigation of SVOC in diesel fuel, engine lubricating oil and diesel engine emissions, Cambridge Particle Meeting, University of Cambridge.

Zhao, Y., Nguyen, N. T., Presto, A. A., Hennigan, C. J., May, A. A. and Robinson, A. L., 2015. Intermediate volatility organic compound emissions from on-road diesel vehicles: Chemical Composition, emission factors, and estimated secondary organic aerosol production, Environ. Sci. Technol., 49, 11516-26.

NOMENCLATURE

Acc.	Accumulation mode (also referred to as soot mode)
Bicyclics	Bicyclic alkanes
BMEP	Brake mean effective pressure
CI	Compression ignition
CLD	Chemiluminescence detection
CLIC	Computer language for identifying chemical
CMD	Count median diameter
CO	Carbon monoxide
CO_2	Carbon dioxide
CPC	Condensation particle counter
DCM	Dichloromethane
DI	Direct-injection
DMA	Differential mobility analyser
DOC	Diesel oxidation catalyst
DPF	Diesel particulate filter
EGR	Exhaust gas recirculation
FID	Flame ionisation detector
GC	Gas chromatography
GC×GC	Two-dimensional gas chromatography
GC×GC-ToF-MS	Two dimensional gas chromatography time-of-flight mass spectrometry
g/kg_f	Grams per kilogram of fuel consumed
HC	Hydrocarbons
HEPA	High-efficiency-particulate-air
H_2SO_4	Sulphuric acid
I+SVOC	IVOC+SVOC
IVOC	Intermediate-volatility organic compounds
mg/kg_f	Milligrams per kilogram of fuel consumed
Monoaromatics	Monocyclic aromatics
MPA	Magneto-pneumatic
MS	Mass spectrometry
Nano-Moudi	Nano-micro orifice uniform deposit impactor
NDIR	Non-dispersive Infra-Red

NEDC	New European driving cycle
NO	Nitrogen monoxide
NO_2	Nitrogen dioxide
NO_x	Oxides of nitrogen
Nuc.	Nucleation mode
O_2	Oxygen
Open-ECU	Open engine control unit
Oxygenates	Oxygenated compounds
PAH	Polycyclic aromatic hydrocarbons
PM	Particle mass
POA	Primary organic aerosol
PSM	Particle size magnifier
RDE	Real driving emissions
RPM	Revolutions per minute
SCR	Selective catalytic reduction system
SOA	Secondary organic aerosol
SVOC	Semi-volatile organic compounds
THC	Total hydrocarbons
ToF	Time of flight
UCM	Unresolved complex mixture
VNT	Variable-nozzle-turbine

869

TABLES LEGENDS

Table 1: Engine specifications.

Table 2: Gaseous emissions characteristics (Red. % means the percentage of decrease of each parameter over the aftertreatment systems).

Table 3: Particle mass (PM) and I+SVOC emissions characteristics.

Table 4: Mass ratio of each class of I+SVOC to the total particle mass (PM).

Table 5: Mass ratio of each class of I+SVOC to the total I+SVOC.

FIGURES LEGENDS

Figure 1: Schematic of the engine test cell.
DAQ refers to the data acquisition board,
* samples were taken before DOC, after DOC and after DOC+DPF.

Figure 2: Schematic of the dilution and sample collection system.
* this flow meter (rotameter) was used to assure flow rates and was removed during sampling

Figure 3: Particle size distribution (a) number and (b) volume at different sampling locations. (Particles with diameter between 1.2 nm and 2.5 nm were measured with the PSM sampling system and particles with diameter between 4.87 nm and 1000 nm (the grey area) were measured with the DMS sampling system).

Figure 4: Total I+SVOC concentrations at different exhaust particle sizes collected by the Nano-Moudi; (a) Before DOC, (b) After DOC, (c) After DOC+DPF (bars represent the concentrations and lines represent conversion efficiencies using DOC (b) and DOC+DPF (c)).

Figure 5: Contour plots of intermediate- and semi-volatile alkane concentrations collected by the Nano-Moudi at different sampling locations.

Figure 6: Concentrations and conversion efficiencies of different types of I+SVOC (collected by the Nano-Moudi) versus their carbon number at different sampling locations (bars represent the concentrations, and lines represent conversion efficiencies using DOC (red lines / lower conversion efficiencies) and DOC+DPF (green lines / higher conversion efficiencies)).

912 **Table 1**: Engine specifications.

Bore (mm)	86.0
Stroke (mm)	94.6
Connecting Rod Length (mm)	155.0
Capacity (cm^3)	2198
Compression Ratio	15.5:1
Injection System	DI Common Rail (Solenoid Injectors)

913

914

915 **Table 2:** Gaseous emissions characteristics (Red. % means the percentage of decrease of each
916 parameter over the aftertreatment systems).

	CO	THC	NO	NO_2	NO_x	CO_2	Exhaust Gas Temperature
	g/kg_f						°C
Before DOC	97.92	19.97	0.83	4.07	4.90	3015	186
After DOC	2.16	7.62	3.06	0.00	3.06	3209	209
After DOC+DPF	0.00	2.33	2.83	0.03	2.85	3228	206
Red. (DOC) %	97.79	61.85	-270.45	99.99	37.49	-6.4	-12.6
Red. (DOC+DPF) %	100.00	88.32	-241.93	99.32	41.74	-7.1	-10.7

917 Exhaust backpressure difference before and after the aftertreatment system was approximately 5.4 mbar.

918

Table 3: Particle mass (PM) and I+SVOC emissions characteristics.

					I+SVOC				
	Total PM	Total I+SVOC	Nuc. PM	Acc. PM	Alkanes	Cyclo-alkanes	Bicyclic Alkanes	Monocyclic Aromatics	Oxygenated Compounds
	g/kg_f								
Before DOC	0.2156	0.1048	0.0094	0.2063	0.0656	0.0122	0.0082	0.0094	0.0094
After DOC	0.1696	0.0265	0.0032	0.1664	0.0115	0.0043	0.0018	0.0014	0.0075
After DOC+DPF	0.0000	0.0089	0.0000	0.0000	0.0045	0.0012	0.0005	0.0006	0.0022
Red. (DOC) %	21.36	74.71	65.84	19.34	82.51	65.09	77.64	84.79	20.08
Red. (DOC+DPF) %	100.00	91.50	100.00	100.00	93.16	90.34	94.37	93.90	76.49

PM is from the DMS sampling system and I+SVOC is from the Nano-Moudi sampling system using the in-house dilution system

Table 4: Mass ratio of each class of I+SVOC to the total particle mass (PM).

	Alkanes	Cyclo-alkanes	Bicyclic Alkanes	Monocyclic Aromatics	Oxygenated Compounds	Total I+SVOC
	%					
Before DOC	30.4	5.7	3.8	4.4	4.4	48.6
After DOC	6.8	2.5	1.1	0.8	4.4	15.6
After DOC+DPF	-	-	-	-	-	-

PM is from the DMS sampling system and I+SVOC is from the Nano-Moudi sampling system using the in-house dilution system

927 **Table 5:** Mass ratio of each class of I+SVOC to the total I+SVOC.

	Alkanes	Cyclo-alkanes	Bicyclic Alkanes	Monocyclic Aromatics	Oxygenated Compounds
	%				
Before DOC	62.6	11.7	7.8	9.0	9.0
After DOC	43.3	16.1	6.9	5.4	28.3
After DOC+DPF	50.4	13.2	5.2	6.4	24.8

928 I+SVOC is from the Nano-Moudi sampling system using the in-house dilution system

929

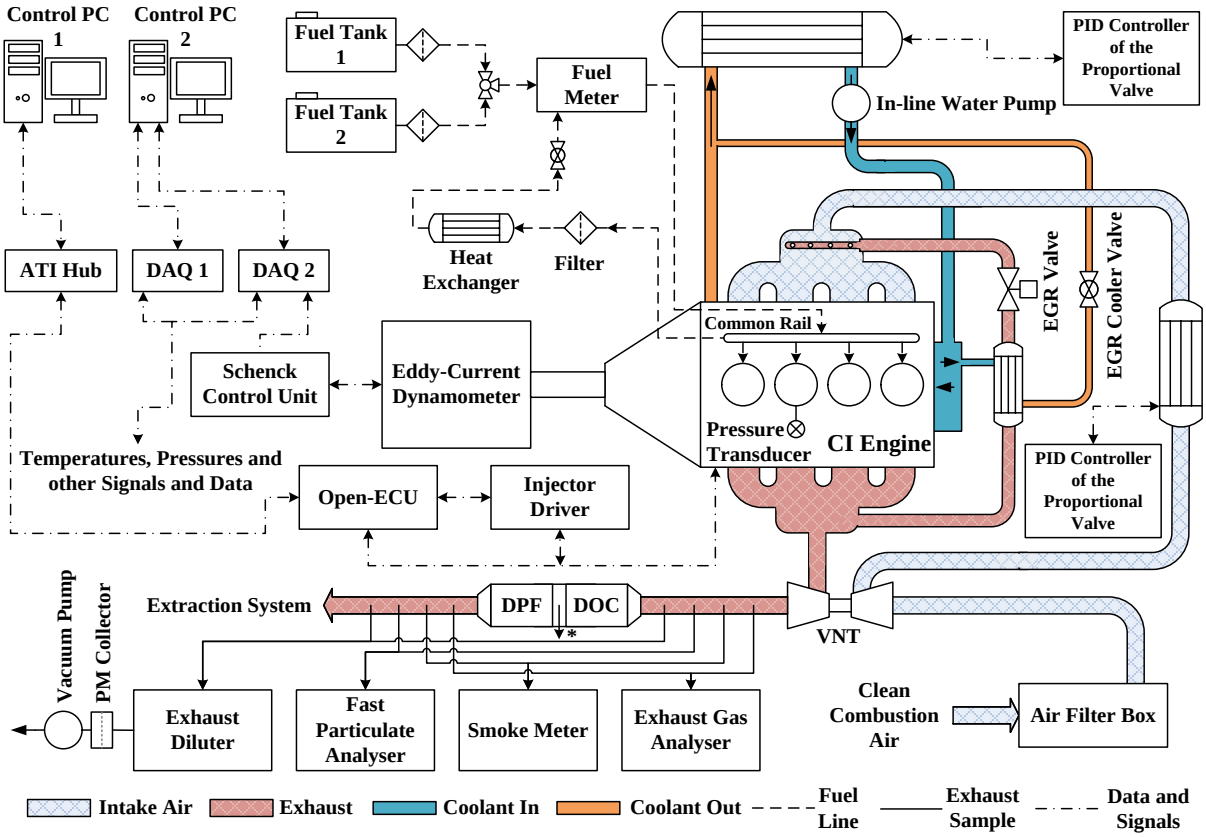

930

931 **Figure 1:** Schematic of the engine test cell.
932 DAQ refers to the data acquisition board,
933 * samples were taken before DOC, after DOC and after DOC+DPF.
934

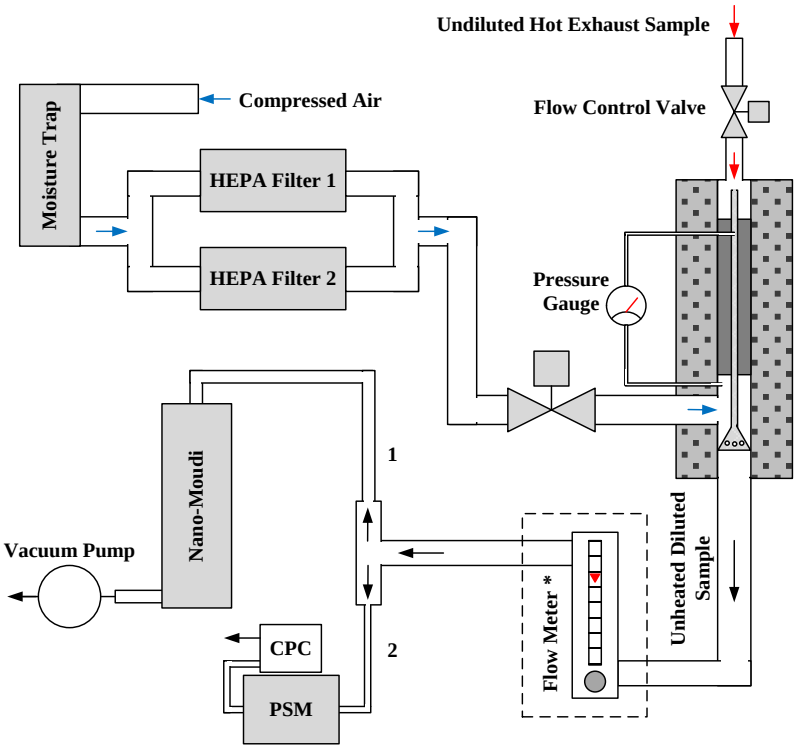

935

936 **Figure 2:** Schematic of the dilution and sample collection system.
937 * this flow meter (rotameter) was used to assure flow rates and was removed during sampling

938

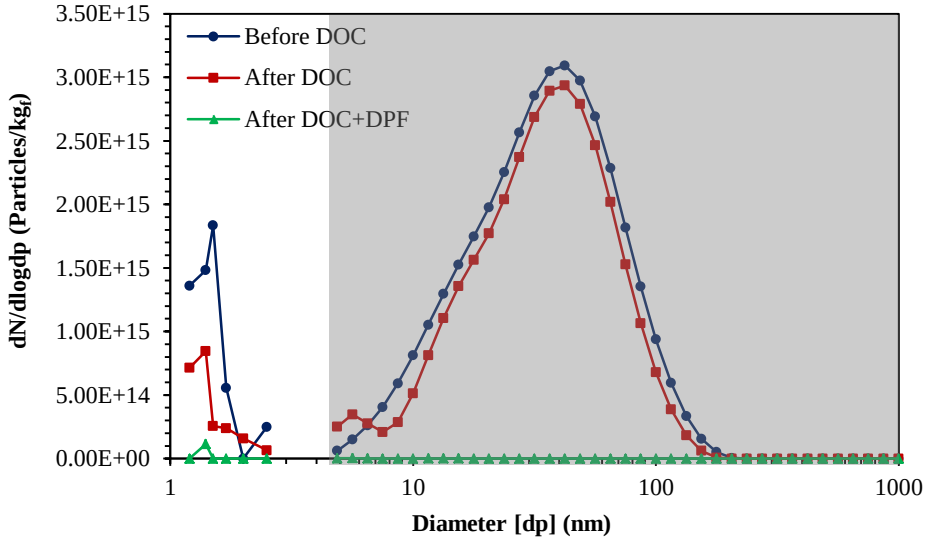

(a)

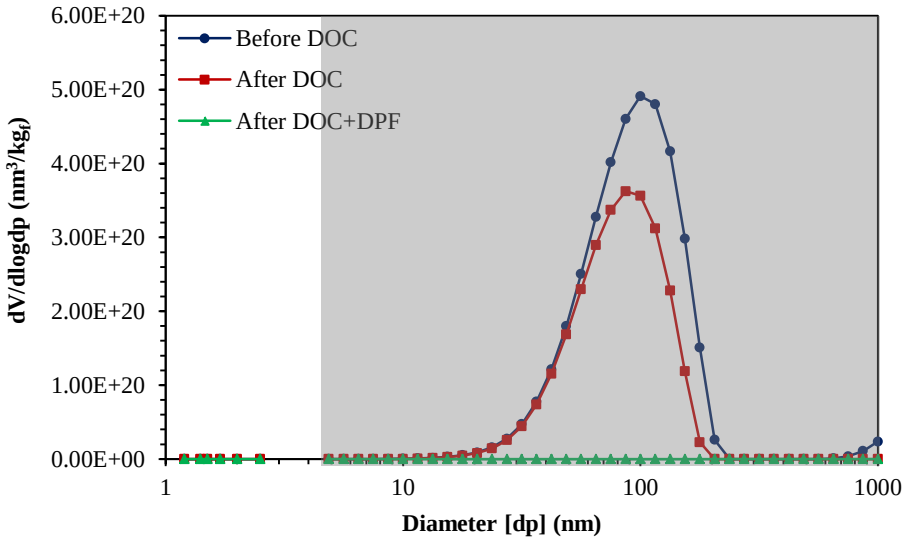

(b)

Figure 3: Particle size distribution (a) number and (b) volume at different sampling locations. (Particles with diameter between 1.2 nm and 2.5 nm were measured with the PSM sampling system and particles with diameter between 4.87 nm and 1000 nm (the grey area) were measured with the DMS sampling system).

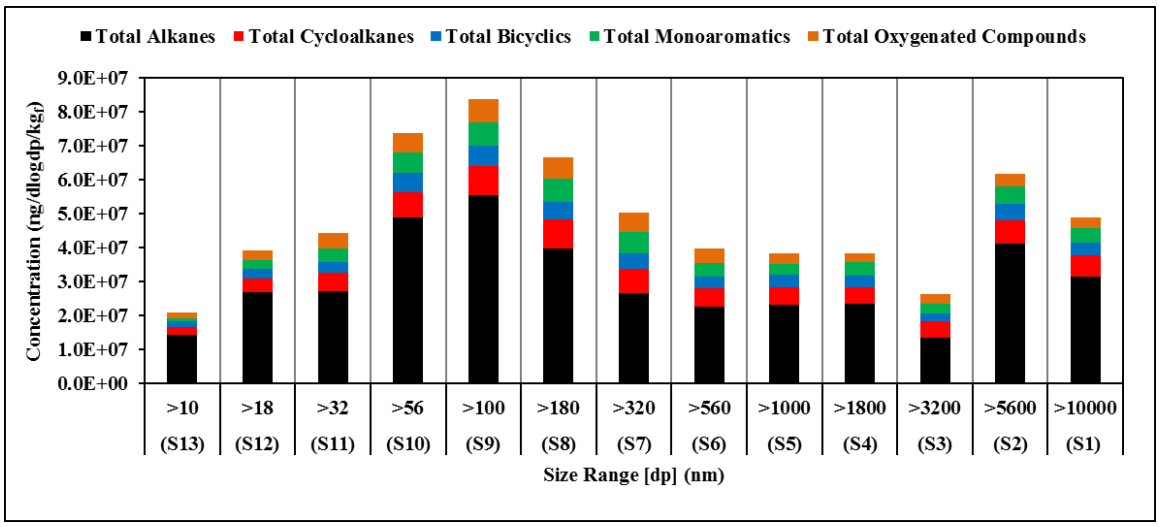

(a)

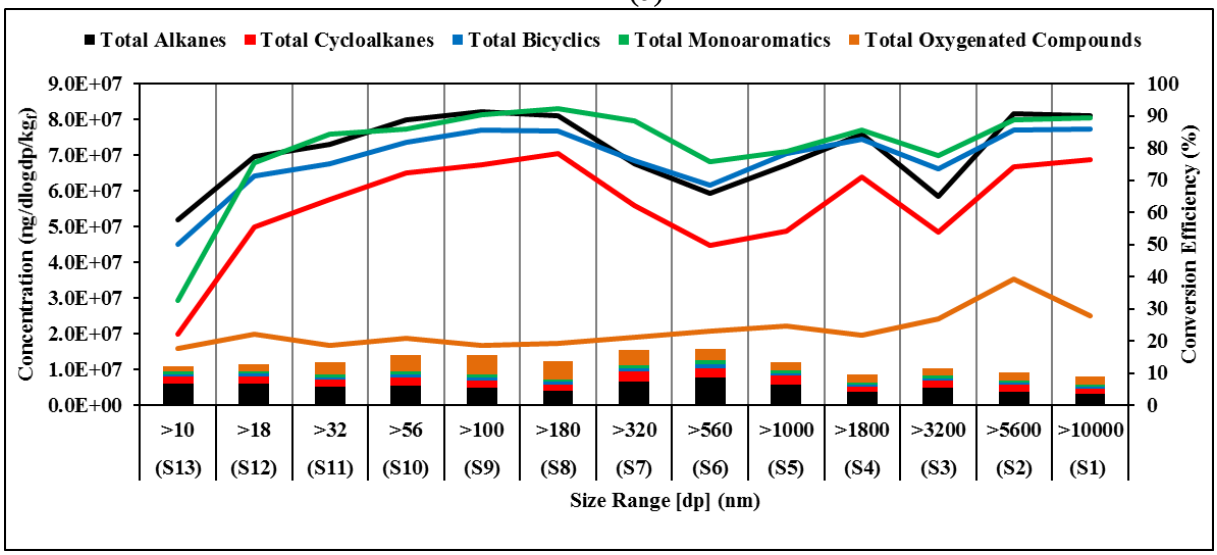

(b)

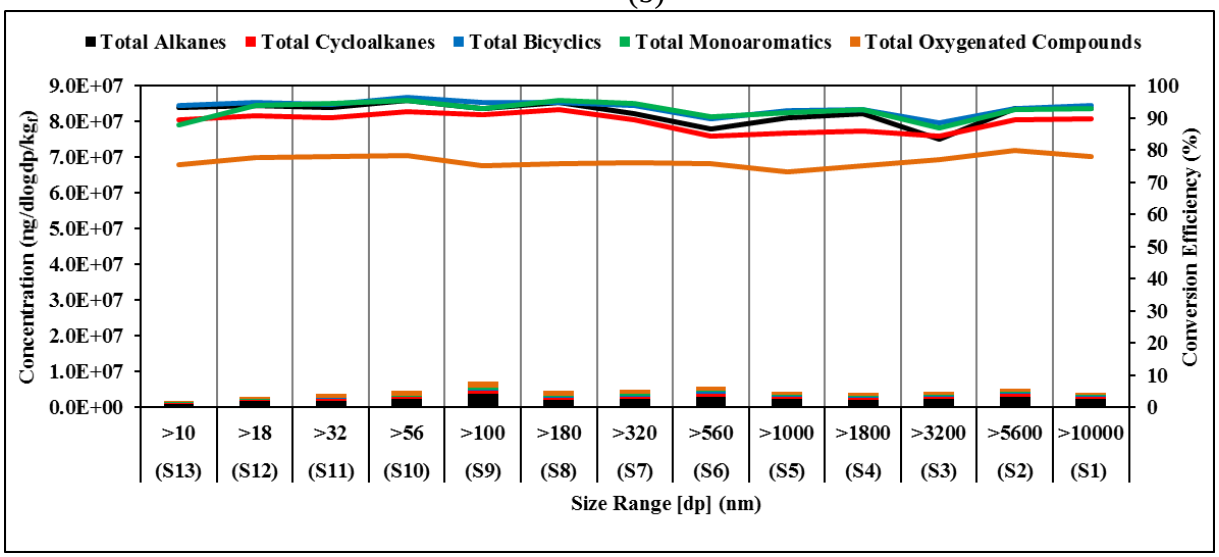

(c)

Figure 4: Total I+SVOC concentrations at different exhaust particle sizes collected by the Nano-Moudi; (a) Before DOC, (b) After DOC, (c) After DOC+DPF (bars represent the concentrations and lines represent conversion efficiencies using DOC (b) and DOC+DPF (c)).

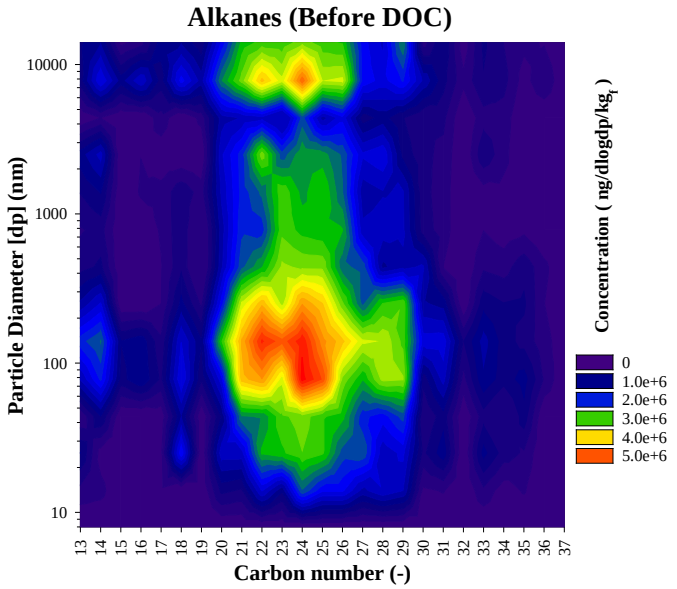

958

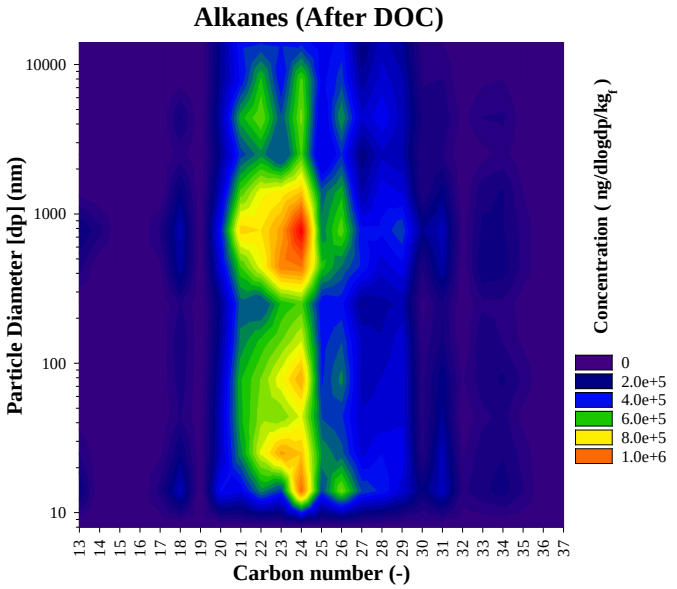

959

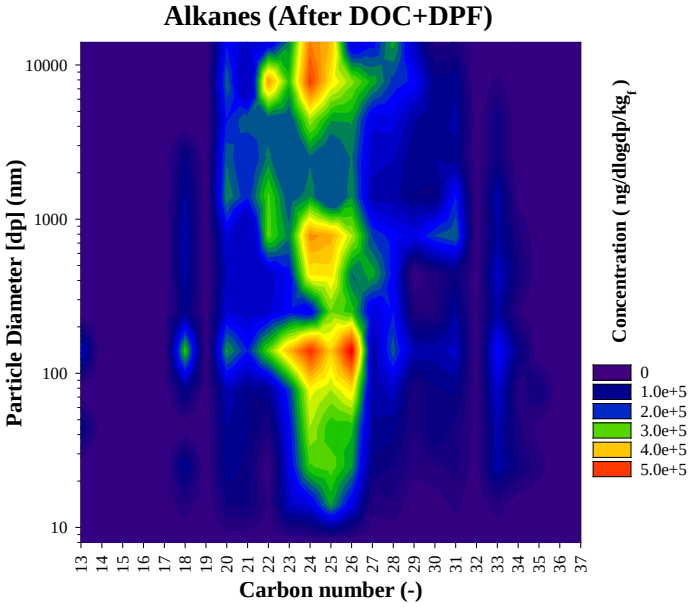

960
961

962 **Figure 5:** Contour plots of intermediate- and semi-volatile alkane concentrations collected by the
963 Nano-Moudi at different sampling locations.

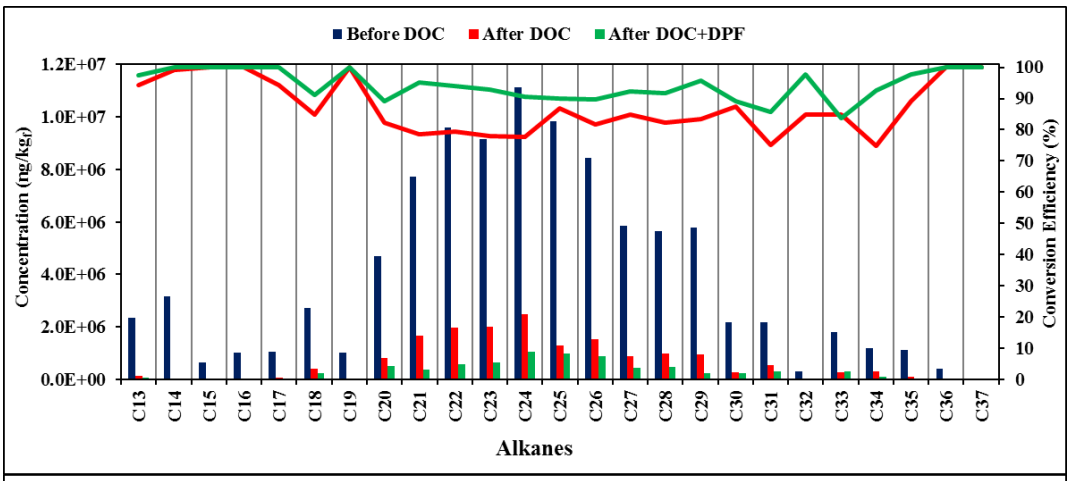

964

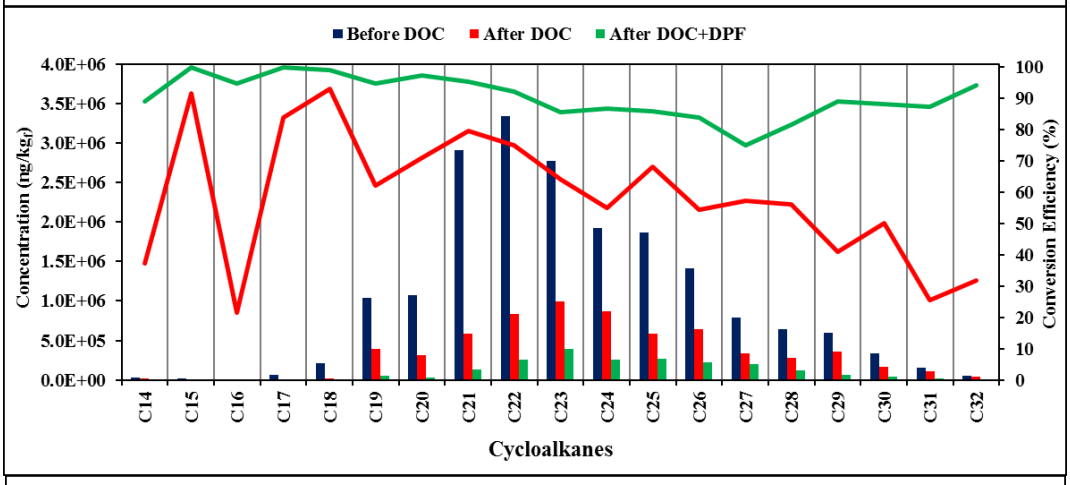

965

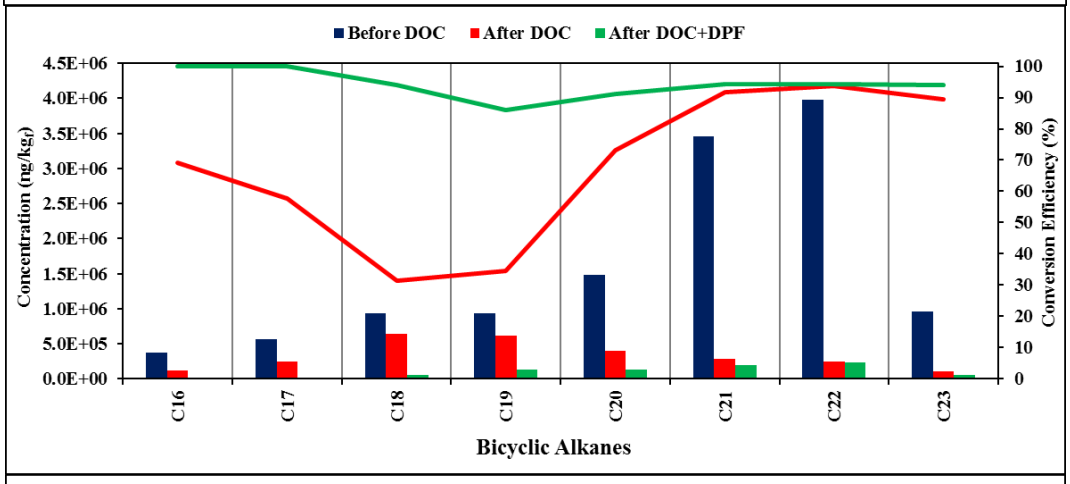

966

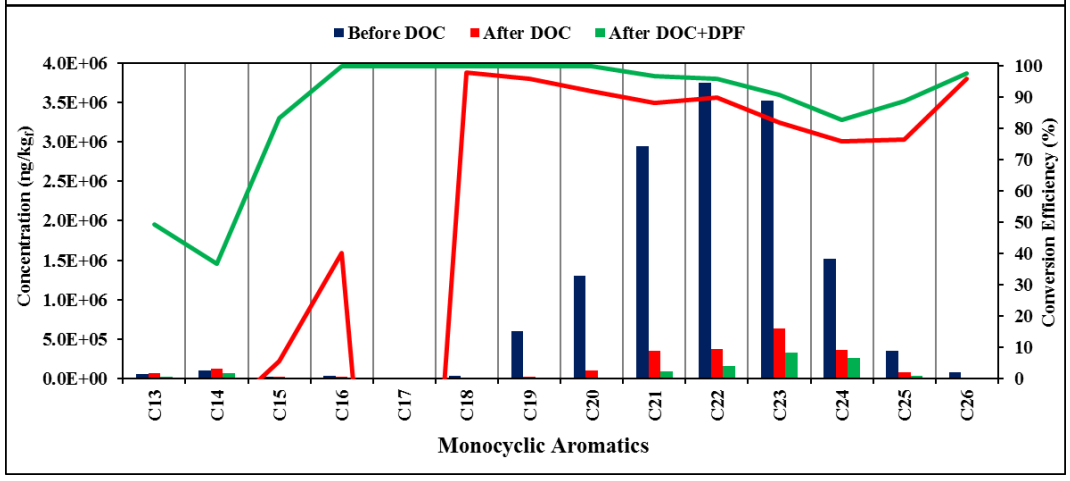

967

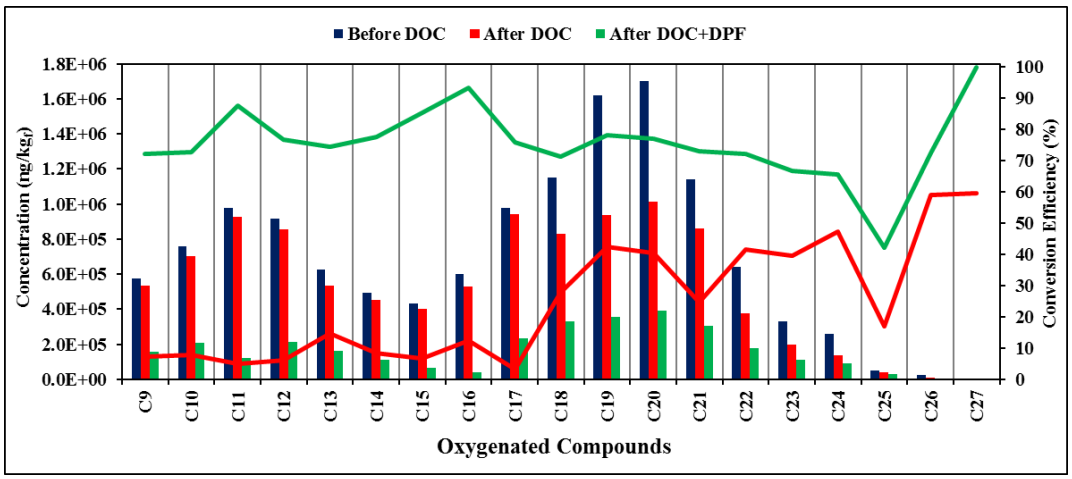

Figure 6: Concentrations and conversion efficiencies of different types of I+SVOC (collected by the Nano-Moudi) versus their carbon number at different sampling locations (bars represent the concentrations,the f and lines represent conversion efficiencies using DOC (red lines / lower conversion efficiencies) and DOC+DPF (green lines / higher conversion efficiencies)).